

# A hyperspectral image projector for hyperspectral imagers

Joseph P. Rice, Steven W. Brown, Jorge E. Neira, and Robert R. Bousquet

Optical Technology Division  
National Institute of Standards and Technology, Gaithersburg, MD, USA 20899

## ABSTRACT

We have developed and demonstrated a Hyperspectral Image Projector (HIP) intended for system-level validation testing of hyperspectral imagers, including the instrument and any associated spectral unmixing algorithms. HIP, based on the same digital micromirror arrays used in commercial digital light processing (DLP<sup>®</sup>) displays, is capable of projecting any combination of many different arbitrarily programmable basis spectra into each image pixel at up to video frame rates. We use a scheme whereby one micromirror array is used to produce light having the spectra of endmembers (i.e. vegetation, water, minerals, etc.), and a second micromirror array, optically in series with the first, projects any combination of these arbitrarily-programmable spectra into the pixels of a 1024 x 768 element spatial image, thereby producing temporally-integrated images having spectrally mixed pixels. HIP goes beyond conventional DLP projectors in that each spatial pixel can have an arbitrary spectrum, not just arbitrary color. As such, the resulting spectral and spatial content of the projected image can simulate realistic scenes that a hyperspectral imager will measure during its use. Also, the spectral radiance of the projected scenes can be measured with a calibrated spectroradiometer, such that the spectral radiance projected into each pixel of the hyperspectral imager can be accurately known. Use of such projected scenes in a controlled laboratory setting would alleviate expensive field testing of instruments, allow better separation of environmental effects from instrument effects, and enable system-level performance testing and validation of hyperspectral imagers as used with analysis algorithms. For example, known mixtures of relevant endmember spectra could be projected into arbitrary spatial pixels in a hyperspectral imager, enabling tests of how well a full system, consisting of the instrument + calibration + analysis algorithm, performs in unmixing (i.e. de-convolving) the spectra in all pixels. We discuss here the performance of a visible prototype HIP. The technology is readily extendable to the ultraviolet and infrared spectral ranges, and the scenes can be static or dynamic.

Keywords: digital micromirror device, hardware-in-the-loop, hyperspectral, image, imaging, multispectral, projector, remote sensing, spectroscopy, testing, video

## 1. INTRODUCTION

The problem of validating the information obtained from hyperspectral or multispectral imaging systems and their retrieval algorithms has traditionally been approached using one or both of two general methods. In the first, either calibrated radiance (or reflectance) or end data products are compared with in-situ field measurements [1,2]. In the second, the algorithms that convert radiance (or reflectance) data cubes to desired end data products are validated through computer-based simulations [3]. The first approach has the advantage that it potentially tests the entire system, which consists of the instrument itself, the counts-to-radiance (or reflectance) calibration, and the product retrieval algorithms, but it can be expensive to implement and its scope must usually be limited. The second can inexpensively test over the entire range of data, but it only validates the algorithms, not the instrument and its calibration. Single-grating or filter-based instruments such as those used in hyperspectral and multispectral imagers are notorious for calibration problems, particularly spectral stray light [2,4], so a full system-level validation is preferable when possible.

We are developing a third, complementary approach that enables inexpensive system-level validation. In this approach, controlled hyperspectral scenes having known values of end data products are projected into the instrument, and the

Correspondence: joe.rice@nist.gov

Property of the United States Government. Not subject to copyright.

measured data cubes and retrieved data products are compared with the known ones. The projected scene can be either computer-generated or derived from a real data cube, and in this sense the new validation approach is similar to the computer-based simulation approach. The point of departure is that in the new approach the scene light is actually projected into the real hyperspectral or multispectral instrument, such that the hardware is in the loop. Thus this approach validates the entire system: instrument, calibration, and retrieval algorithms, while retaining the ability to inexpensively test over the range of data without requiring field campaigns. While the general idea of this approach is not new to the hardware-in-the-loop community, where spatial images are routinely projected, the concept of including realistic spectra in every spatial pixel to better simulate reality has not typically been applied yet.

The new technology that will enable this approach is the Hyperspectral Image Projector (HIP) [5-8]. The HIP projects a programmable spectrum into each spatial pixel of an image. That is, the HIP projects hypercubes, not just the red-green-blue (RGB) images of traditional color projectors and displays. Just how this is done is described below. Then this projected scene can be viewed alternately by the instrument under test (IUT, i.e. the hyperspectral or multispectral imager) and a well-calibrated reference instrument. The data cube measured by the IUT can then be compared to that measured by the reference instrument, which measures the truth data cube, for a validation of the IUT and its calibration. Furthermore, the projected hypercube can be designed to include particular *a priori* known values for the end data products: for example, a spectral and/or spatial signature of interest, for which the IUT and its retrieval algorithm is supposed to be able to detect. The degree to which the IUT system, including its radiance or reflectance calibration, and its correction and retrieval algorithms, can actually detect the signature then constitutes a system-level validation test.

In this paper we provide a brief status report of our HIP development. First, we provide a brief description of the design and operation of our visible-band prototype. Then, we describe an algorithm for radiometrically efficient projection of a real data cube. From this we determine a set of realistic endmember spectra that are to be simulated and projected by HIP, so we discuss our current spectral matching algorithm and present the results.

## 2. HIP PROTOTYPE

### 2.1. Design and Operation

The schematic of a prototype HIP that we have built on a breadboard is shown in Fig. 1. It consists of a spectral engine coupled to a spatial engine. The spectral engine produces a series of programmable spectra, which we call basis spectra. The spatial engine maps them in the correct proportions, such as determined by a corresponding set of spatial images that we call spectral planes (a generalization of color planes). For those familiar with hyperspectral imaging terminology, the basis spectra can be thought of as endmember spectra, and the spectral planes can be thought of as abundance images.

The spectral engine works as follows. Light from a Xe arc source is fed through a liquid light guide (not shown), collected by lens L1, focused by lens L2 through the entrance slit, and collimated by lens L3 onto Prism1, as in a spectrograph. Lenses L2 and L3 are cylindrical and oriented to focus to a line parallel to the slit (perpendicular to the page). The spectrally dispersed output of Prism1 is imaged by lens L4 onto a digital micromirror device (DMD\*) having 1024 columns and 768 rows, such that each of the DMD columns corresponds to a different wavelength over the spectral range, roughly  $\lambda_1 = 720$  nm to  $\lambda_2 = 410$  nm. At any instant in time, the binary spectral image sent to DMD1 from the personal computer (PC) determines which DMD micromirrors are “on” and which are “off.” “On” micromirrors are tilted clockwise (+12° about the micromirror diagonal) from the DMD normal and thereby reflect the light towards M1. “Off” micromirrors are tilted counterclockwise (−12° about the micromirror diagonal) from the DMD normal and thereby reflect the light into Beam Stop 1. To a first order approximation, the fraction of the 768 micromirrors in each DMD column that are “on” determines the relative spectral intensity at the wavelength corresponding to that column [5-8]. Mirror M1 collects the light from these on-state DMD micromirrors and collimates it onto Prism2. This prism is oriented such that spectrally dispersed light is re-combined spatially, such as in a double subtractive spectrograph. Lens L5 then focuses the output of the spectral engine to a spot having a diameter of about

5 mm, for coupling into the spatial engine. L1, L4, and L5 are all spherical lenses, and the prism material is SF10 for both prisms. These optics are anti-reflection coated for the visible wavelength range.

The spatial engine works as follows. The spot of light from the spectral engine is first passed through a homogenizer consisting of four plane mirrors forming the walls of a rectangular tunnel. Through multiple internal reflections as the light propagates along the open length of the homogenizer, the circular, spatially-non-uniform input spot is transformed into a relatively uniform beam having a rectangular cross-section matching the 4:3 aspect ratio of DMD2. This, together with the Illumination Optics, the Fold Mirror, and lens L6 serves to provide spatially uniform illumination of DMD2. DMD2 has 1024 columns (samples) and 768 rows (lines). The PC loads the 8-bit grey scale spectral plane (abundance image) onto DMD2 that corresponds to the basis spectrum (endmember spectrum) of DMD1. The on-state mirrors of DMD2 then display this spatial image during the display time of the binary spectral image on DMD1, and L6 and the Projection Optics focus a magnified image of the DMD2 image onto a white diffuse Projection Screen. Unwanted light from off-state mirrors is captured by Beam Stop 2. Both the Illumination Optics and the Projection Optics are multiple-element lenses in our prototype, designed to provide high quality imaging, while the rest of the lenses in Fig. 1 are currently single elements. All of the lens optics, and the DMD windows, are anti-reflection-coated for the visible wavelength range. As shown in Fig. 1, the Projection Optics provide an offset, keystone-corrected image such that the IUT can be mounted normal to the projection screen. While the offset shown in Fig. 1 appears to be horizontal, it is actually vertical (out of the page) in our prototype. Instead of using a projection screen, it is of course possible, and in many cases preferable, to directly-couple the DMD2 spatial image to the IUT using, for example, a collimator. We are working on that arrangement. However, the current prototype that we discuss in this paper is as shown in Fig. 1.

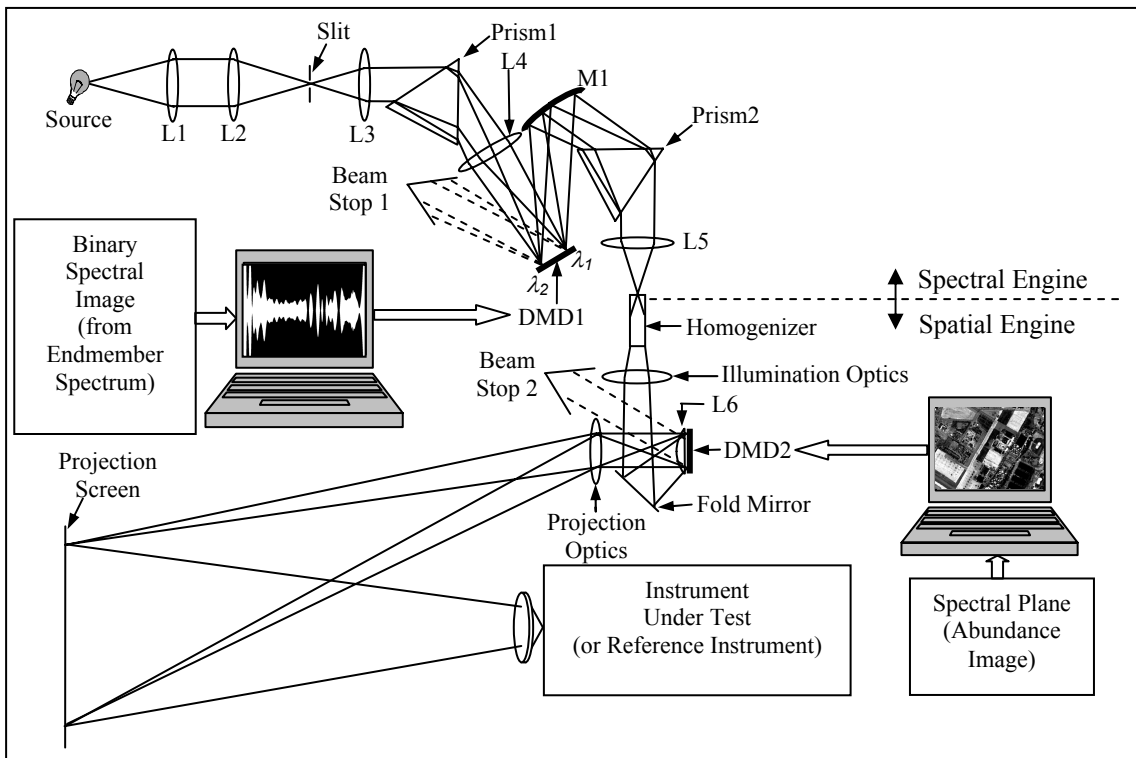


**Figure 1.** Schematic of the Hyperspectral Image Projector prototype. Endmember spectra are displayed on DMD1 in sync with the display of the corresponding abundance images on DMD2. The DMDs are shown edge-on in this schematic. The full set of endmember spectra and abundance images are displayed within the integration time of the instrument under test, which then measures the projected hyperspectral image. (Though two computers are shown here for illustration purposes, in practice only one computer is used).

The HIP then works as follows. Both DMDs display their respective images in sync with a 5 V trigger pulse. Successive pulses trigger the display of the successive basis spectra on DMD1 and corresponding spectral planes on DMD2. The complete set of spectral planes is displayed within the integration time of the IUT. Consider a hyperspectral or multispectral IUT based upon a 2D staring focal plane array, focused on the projection screen with 1:1 mapping of projector pixels to IUT pixels, and consider the ideal situation in which aberrations, aliasing, air transmittance, and other contaminating effects are ignored. During its integration time, each pixel of this IUT would then be exposed all endmember spectra in proportion to the corresponding pixels of the abundance images, and upon integration would measure the counts from that pixel as if it had been reflected from the real scene from which the basis spectra (endmember spectra) and spectral planes (abundance images) were derived. While there are, in reality, several contaminating effects to be properly dealt with, to first order the HIP is indeed capable of simulating reality in that every pixel can have any spectrum.

## 2.2. Spectral Engine Calibration

Wavelength calibration was achieved by temporarily swapping the spatial engine with a 10 cm diameter Spectralon integrating sphere coupled to a calibrated array spectrometer. The output from the spectral engine was directed into a 2.5 cm diameter entrance aperture of this integrating sphere, and its spectrum was measured with the spectrometer. Sixteen line spectra, spanning the full spectral range of the prototype HIP, were generated one at a time by the spectral engine and measured by the spectrometer. Each line spectrum was generated by turning on all mirrors of 10 contiguous DMD1 columns, with all other DMD1 mirrors off. Examples of the resulting lineshape data are shown in Fig. 2a, and are for an entrance slit width of 250 micrometers. The slightly asymmetric lineshapes resulted mainly from the imperfect imaging quality of lens L4 of the dispersed spectrum onto DMD1. This led to some distortion of the spectral image, such that contours of constant wavelength were not straight vertical lines as in the ideal situation, but were curved over ten or so DMD1 columns. There is also significant stray light in this prototype spectral engine, as can be seen in these line spectra. The data points from each line spectrum having values greater than 80% of the peak were fit by Lorentzian functions, which enabled determination of the center wavelength for each spectrum in a way relatively insensitive to distortion and stray light. Then, a fourth-order polynomial was used to fit the corresponding DMD1 column numbers to these center wavelengths, as shown in Fig. 2b, and a look-up-table (LUT) was computed from this fit for mapping wavelength to DMD1 column number for all subsequent spectra to be displayed. The nonlinear relationship in Fig. 2b results from the use of a prism as the dispersion element, and this process corrects for that

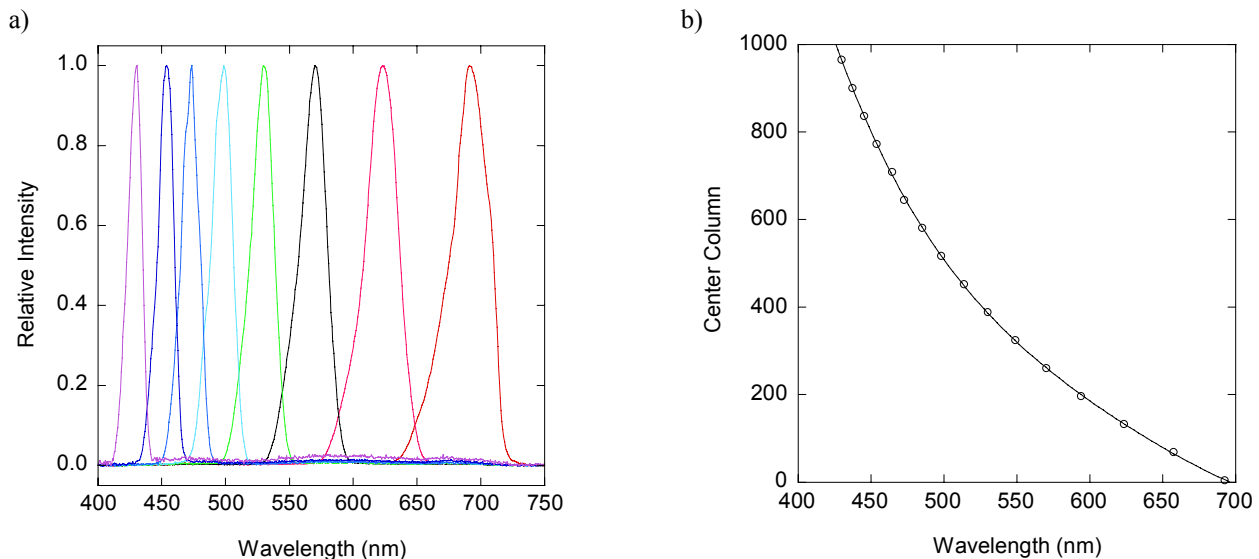


**Figure 2.** a) Wavelength calibration of the prototype HIP spectral engine with contiguous sets of DMD1 columns turned on, one at a time, spanning DMD1. Only eight spectra are shown for clarity. b) The center wavelengths of each line spectrum are plotted as open circles, and the solid line is a fit of these data by a fourth-order polynomial, used subsequently to produce a wavelength calibration look-up-table giving the DMD column corresponding to each wavelength.

nonlinearity to within a fitting uncertainty of about 1 nm ( $k=1$ ). The entire process is automated using LabVIEW software that we have developed, and because of the speed of the DMD, the array spectrometer, and the PC, only takes a few seconds.

The overall relative spectral intensity of the spectral engine with all DMD1 mirrors on was also measured, again using the integrating sphere and spectrometer, and is shown in Fig. 3. The line structure is inherent in the Xe arc source, and will become important below when we discuss spectral matching. These data also show that the useable spectral range of this prototype is 450 nm to 670 nm. This range can of course be changed by modifying the optics, as the inherent Xe arc source spectrum is much broader than this.

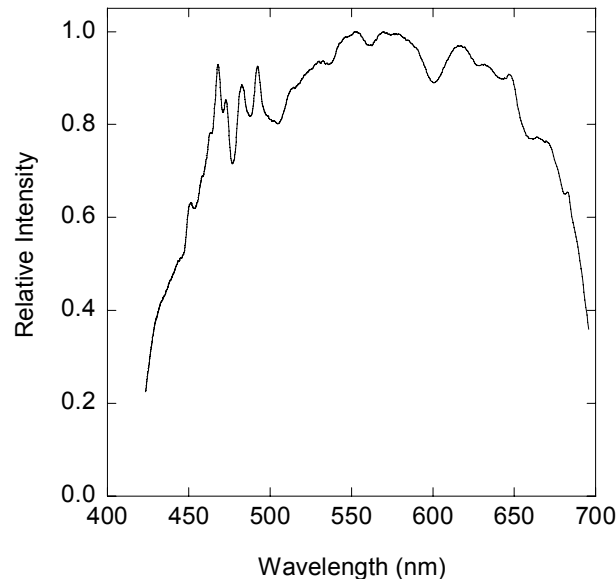


**Figure 3.** Relative intensity calibration of the prototype HIP spectral engine with all DMD1 mirrors on. This is called the Full Intensity spectrum below. The features between 450 nm and 500 nm are characteristic of the Xe arc source.

While other characterizations show that the intensity varies along the DMD1 columns, falling off by about a factor of two from the center to the top or bottom, this effect has not been explicitly corrected for in the results reported here. Rather, the approach used here was to let this intensity variation effect and the stray light effect mentioned above be corrected implicitly during the spectral matching discussed in Section 4.

### 3. ALGORITHM FOR PROJECTION OF A REAL DATA CUBE

In the previous section we addressed the question of how to project a hyperspectral data cube on HIP. In this section we discuss the question of what to project. Specifically, given that HIP can project real hypercubes, what must be done to prepare a data cube for efficient projection on HIP? In answering this, we use the data cube represented by the image of Fig. 4 as an example. This is a calibrated and corrected reflectance image of the North Island Naval Air Station (NAS) in San Diego, California, as measured by the Airborne Visible/Infrared Imaging Spectrometer (AVIRIS), an aircraft-based hyperspectral imager measuring from 400 nm to 2500 nm using 224 contiguous spectral bands [9]. The RGB image in Fig. 4 uses Band 28 (635.72 nm) for the red color plane, Band 19 (547.32 nm) for the green color plane, and Band 10 (458.89 nm) for the blue color plane.

In order to prepare this data cube for projection on HIP, we first used commercially-available Environment for Visualization of Images (ENVI) software to resize the spatial dimensions of the data to 1024 x 768, from an original 400 x 400 source data cube, including only a spatial subset of the original data to maintain square pixels. Fig. 4 shows

this spatial subset, chosen because it has a range of materials, as well as a few aircraft. This resizing step was performed so that the data cube matched the HIP prototype spatial resolution of 1024 x 768. Also, we used the contiguous spectral subset of the data consisting of Band 9 (449.06 nm) through Band 41 (730.49 nm), a total of thirty bands (There were no bands having numbers 33, 34, and 35 in the source data cube, but Bands 32 and Band 36 are contiguous). This spectral subset was used since it corresponds roughly to the spectral range of the HIP prototype.



**Figure 4.** Example image measured by the AVIRIS hyperspectral imager of the North Island Naval Air Station in San Diego, CA.

At this point we could use HIP to project a set of thirty monochromatic line spectra, each centered on an AVIRIS band, and projected one after the other. The intensity of each of these projected monochromatic line spectra could perhaps be adjusted to match the AVIRIS response in each band at each spatial pixel, which is already directly encoded in the thirty spectral planes that constitute our example data cube. All thirty line spectra would be projected by the HIP spectral engine within the integration time of the IUT, in sync with the projection of the corresponding spectral planes on the HIP spatial engine. This would be using the HIP in what we call monochromatic projection mode. However, this would not be the most efficient projection algorithm in terms of projector brightness level, since most of the time an unnecessarily large proportion of the available light would be rejected rather than projected.

It is radiometrically more efficient to use HIP with a broadband projection algorithm, where the multiplex advantage inherent within HIP can be utilized. In broadband mode, we project a smaller set of broadband basis spectra, sampled appropriately for each spatial pixel according to a corresponding set of spectral planes. Since we will have fewer spectral planes, the IUT can spend a larger fraction of its integration time on each one. Also, since the spectra are broadband, the IUT spectral bands are stimulated in a more parallel manner, as opposed to being stimulated in series as in the monochromatic projection mode. This is the multiplex advantage of broadband mode projection.

In order to use a broadband projection algorithm, first we have to determine this reduced set of broadband basis spectra and the corresponding spectral planes from our thirty-band data cube. For this work we used the Sequential Maximum Angle Convex Cone (SMACC) algorithm, which was reported at this same conference three years ago [10]. ENVI now includes SMACC as a standard routine. This algorithm automatically finds endmember spectra from the data. The spectra from a few pure pixels match the endmember spectra. The spectra of the vast majority of pixels in the scene will not match any one endmember spectrum alone, but will match a linear combination of the endmember spectra. For a given endmember, the corresponding image that gives the proportion of that endmember spectrum included in each pixel is called the abundance image. The ENVI SMACC routine not only finds the endmember spectra, but it also determines the abundance image corresponding to each endmember spectrum. The endmember spectra then become our sought-after HIP basis spectra. Similarly, the corresponding abundance images become the sought-after HIP spectral planes.

We ran the automatic SMACC routine within ENVI on our resized, thirty-band data cube. In the process, we constrained SMACC to sum the endmember abundances to unity. Within twenty seconds of run time on a typical modern laptop PC (2.16 GHz clock rate, 2 GByte random access memory), SMACC reduced our example thirty-band

data cube to the seven endmember spectra shown in Fig. 5, and generated the corresponding seven abundance images having a spatial resolution of 1024 x 768, shown in Fig. 6. The grey level for any pixel in any abundance image indicates the proportion of the corresponding endmember spectrum required to match the data for that pixel. We checked that the values derived for the seven abundances for any pixel indeed sum to unity, as requested by our applied constraint. All spectra in Fig. 5 are reasonable and can be produced by the HIP spectral engine except for Endmember 2 (EM2). This spectrum goes negative at some wavelengths, whereas the HIP spectral engine can only supply positive amounts of light. As it turns out, the magnitude of the Endmember 2 spectra, as shown in Fig. 5, is very small relative to all of the other spectra. Thus Endmember 2 can be omitted with negligible effect on the realism of the scene. Also, remember that we will be measuring the output of the HIP using our reference radiometer (Fig. 1), so omission of anything, while it may affect realism, does not affect accuracy of our knowledge of what we will be projecting into the IUT. The result is that we now have six broadband basis spectra and six corresponding spectral planes. We have effectively reduced the dimensionality of the example data set from thirty to six.

Note that the SMACC endmember spectra may not necessarily correspond with material spectral library data, nor do they need to for HIP. In this case, though, Endmember 4 is approximately similar to what one would expect from vegetation, with the characteristic peak in the green part of the spectrum and large reflectance edge beginning as the near-infrared is approached. Note that the bright regions of the Endmember 4 abundance image correspond, as expected, with the green part of the RGB image in Fig. 4. Note also that the airplanes stick out quite clearly in the Endmember 1 abundance image.

We stress that the application of SMACC to reduce the dimensionality of our data cube is nothing new, nor is SMACC the only algorithm or approach capable of solving this problem. The new aspect is the use of SMACC to prepare images for hyperspectral image projection with HIP. This seems to be a good fit at this point in our HIP development.

After performing the matching step for each spectrum (to be described below in Section 4), we can load the six spectral images (Endmember Spectra 1, 3-7) into HIP spectral engine on-board memory, and we can load the six spectral planes (Abundance Images 1, 3-7) into HIP spatial engine on-board memory. Trigger pulses to the spectral engine and spatial engine then synchronize the display of all six spectral planes during the integration time of the IUT, which performs the required summation.

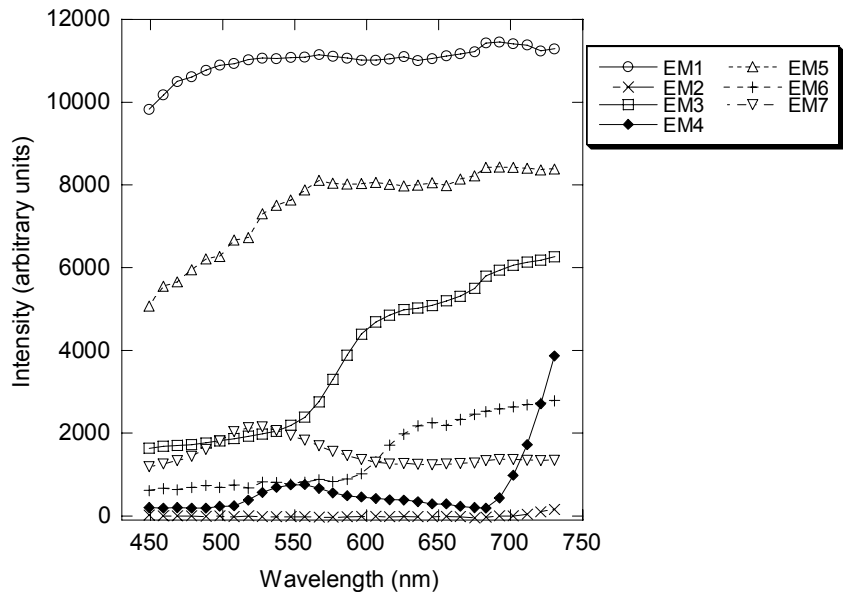


**Figure 5.** Endmember (EM) spectra derived from the North Island Naval Air Station data cube using the ENVI SMACC algorithm. The symbols are the thirty wavelength samples at the AVIRIS original band centers. The lines are guides for the eye. While the absolute intensity scale is arbitrary, the relative scale between the spectra is fixed.

Currently we have developed LabVIEW software for automatically performing these tasks on the prototype HIP. We have demonstrated image projection of three spectral planes derived from standard color Tagged Image File Format (TIFF) images, to provide the proof of principle. We are currently upgrading the LabVIEW software to enable automatic projection of a larger number of spectral planes such as required here (six for this example), a straightforward extension. Ref. 5 discusses details about the number of spectral planes ultimately possible, and explores the related tradeoffs with IUT integration time and required intensity resolution. It also explores other projection formats and extension of this projection technology to the infrared.

#### 4. SPECTRAL MATCHING

We used the following iterative algorithm, fully automated with LabVIEW software that we have developed, to match the measured spectral engine output spectrum to that of a Target spectrum. First, an Aim spectrum is computed that is equal to the Target spectrum for the initial iteration, but will be updated in subsequent iterations. The corresponding binary spectral image is generated from the Aim spectrum using the wavelength calibration LUT (Fig. 2b) and the Full Intensity spectrum (Fig. 3). The algorithm computes the ratio of the Aim spectrum to the Full Intensity spectrum, re-sampling both spectra to 1024 wavelengths as necessary. Wavelength values are then mapped to DMD1 column numbers according to the LUT, and relative intensity values are linearly mapped to the number of “on” pixels at each wavelength. In reality, the intensity varies along any given column of DMD1 since the illumination is not perfectly spatially uniform along the slit direction, so the linearity assumption is not strictly valid. The matching algorithm will correct for this, and to help it initially we start with pixels along the horizontal line at the center of the array, a choice that provides top/bottom symmetry because of the anticipation that the illumination, while non-uniform, is at least peaked near the center. Thus the top half of the all binary spectral images considered here looks like a plot of the Aim/Full spectrum, and the bottom half looks like the Aim/Full spectrum reflected about a horizontal line down the middle of the image.

Upon display of the initial binary spectral image on DMD1, the Measured spectrum is then acquired using the same spectrometer and integrating sphere at the output of the spectral engine that was used for the calibration (Section 2.2). The Measured spectrum is compared to the Target spectrum by computing a Difference spectrum, Measured - Target. For this step, both spectra are re-sampled to a common grid of wavelength values over the range of useable intensity, which was 450 nm to 670 nm for the example measurements below, and each spectrum is normalized to its mean intensity value over this range.

In practice, the initial Measured spectrum does not match the Target spectrum exactly, due not only to the non-uniform illumination discussed above, but also due to spectral engine stray light, slight misalignments, optical aberrations, and diffraction. Thus the matching algorithm uses negative feedback to iteratively adjust the Aim spectrum (and hence the spectral image) to drive toward a Measured spectrum that matches the Target spectrum. If the Target spectrum is denoted as array  $T$ , the Aim spectrum as array  $A_i$ , the Measured spectrum as array  $M_i$ , and the Difference spectrum as array  $D_i$ , the matching algorithm can be expressed as

$$A_0 = T \quad (1)$$

$$D_i = M_i - T \quad (2)$$

$$A_i = A_{i-1} - pD_{i-1} \text{ for } i > 0, \quad (3)$$

where  $i$  is the iteration index and  $p$  is the proportional gain, representing the magnitude of the negative feedback change per iteration. The iteration process is continued until subsequent iterations yield no further improvement to the match. Then the final matched spectral image is saved to disk on the PC until needed later during HIP image playback. The DMD driver electronics and the array-based spectrometer used in the HIP prototype are capable of performing display and measure iterations very rapidly. For the data presented here the matching process was intentionally slowed down to about one iteration per second to enable us to monitor it.

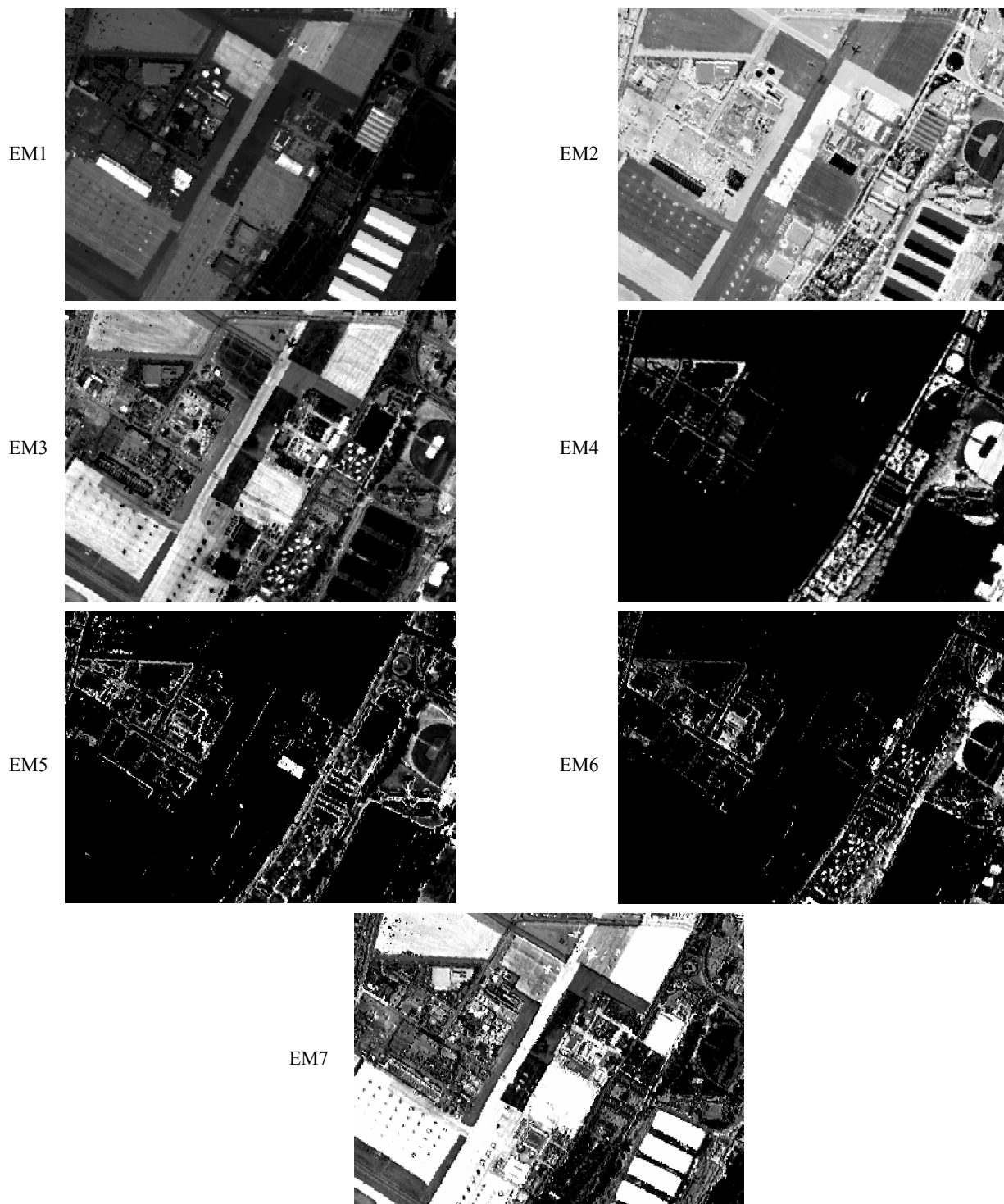


**Figure 6.** Abundance images corresponding to the endmember spectra of Fig. 5, also from SMACC. A contrast stretch has been applied to the grey scale of each of these images to optimize human viewing, and the images have been resized to fit on the page. The actual abundance images sent to the HIP spatial engine retain the grey scale determined by SMACC and are maintained at the 1024 x 768 spatial resolution as required by the HIP spatial DMD2.

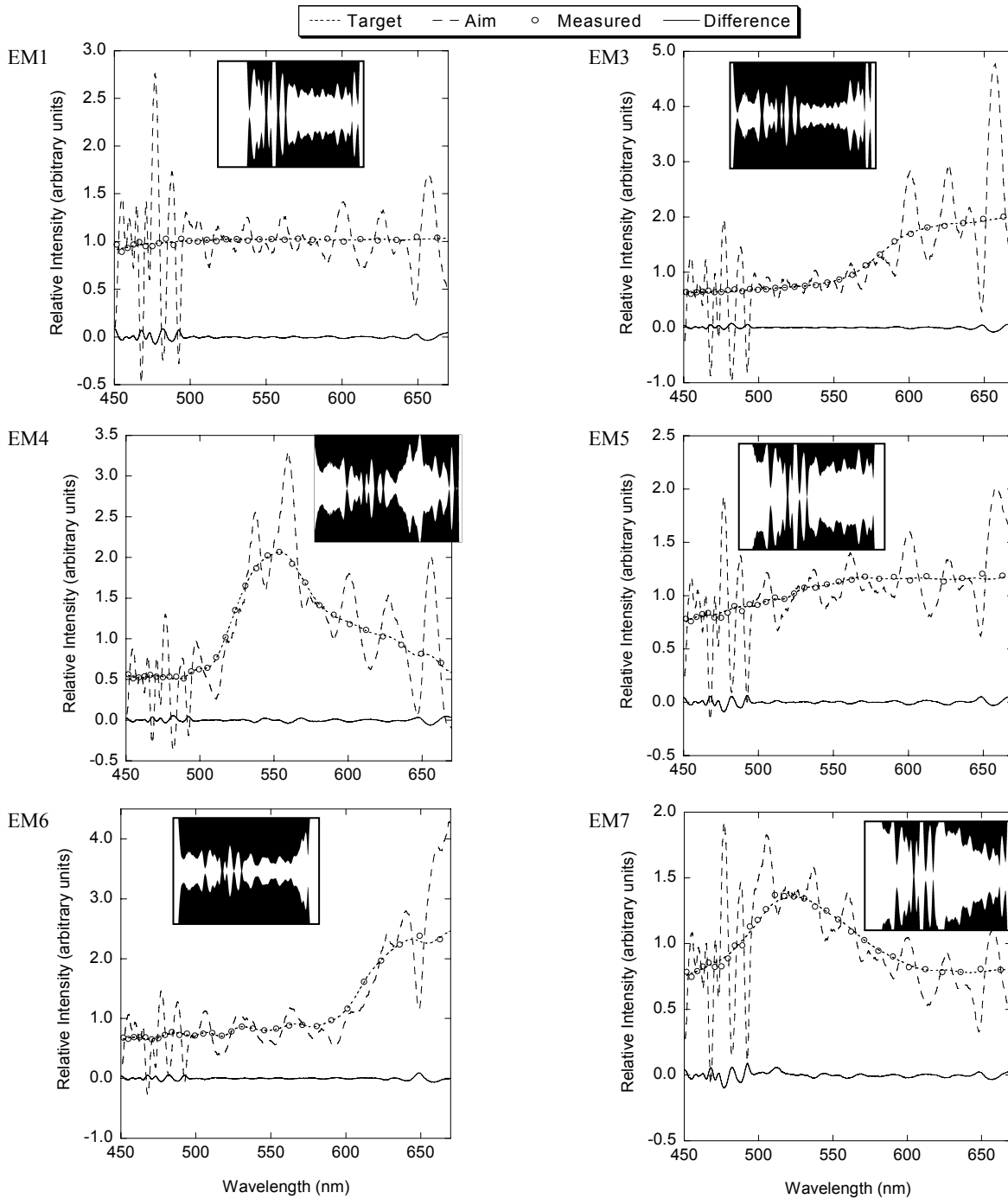


**Figure 7.** Spectral matching results for the six endmember spectra on the prototype HIP. The legend at the top applies to all plots in this figure. Each inset image is the corresponding binary spectral image derived from the Aim spectra and that, when displayed on DMD1, provided the Measured spectra. The spectral images have been flipped horizontally in this figure, so that shorter wavelengths are on the left as in the plots. The Difference spectra are Measured – Target. For each plot, the Target, Aim, and Measured intensity values have been normalized such that the mean across the spectrum is one. To allow the Target and Measured data to both be seen in these plots, only thirty out of the 1024 Measured spectra points have been plotted. However, all 1024 points have been included in the Difference spectra for high-resolution comparison. The other spectra are plotted as lines without data points.

Our spectral matching results for the six endmember spectra (Fig. 5) required to project the North Island Naval Air Station data cube are shown in Fig. 7. For these results, we used  $p = 0.1$  and obtained the matches shown within about 100 to 200 iterations. The residual standard deviation of the difference spectra was typically about 2% of the peak value for these spectra. The largest residual differences are where the Aim spectra compensate for the source spectrum variations, and are within the spectral resolution of the spectral engine. The Aim spectra actually changed by a relatively large amount as the matching algorithm iterated, and the resulting final spectral images have developed large sub-resolution excursions. This indicates how hard the simple matching algorithm works at trying to correct the effects of stray light, misalignments, and optical aberrations in the prototype spectral engine.

Finally, remember that we do not necessarily require a perfect match to the basis spectra, or even to necessarily accurately project the realistic data cube. The requirement for our validation approach is to project scenes that *are close to* possible realistic scenes that the IUT will measure during its use. This is because our validation approach relies on the reference instrument in Fig. 1 to provide us with the truth data cube in the end. In other words, for IUT performance validation we generally do not have as stringent requirements on *control* of the projected hypercube as we do on the *knowledge* of the projected hypercube, and it is the reference instrument that provides us with that knowledge.

## 5. SUMMARY

We have described a prototype Hyperspectral Image Projector that we have built as a test bed for a new approach for system level hardware-in-the-loop style validation of hyperspectral and multispectral imagers as coupled to their retrieval algorithms. Then we introduced the concept of using the SMACC algorithm for automatic dimensional reduction to prepare real data cubes for projection with HIP in broadband mode, and provided a detailed example, including spectrally matching the endmember spectra. We have demonstrated the prototype HIP for projection of three spectral planes, such as standard RGB images. Our next step will be to perform a straightforward upgrade to the software that will enable an arbitrarily large number of spectral planes to be projected.

## ACKNOWLEDGEMENTS

This work was funded in part by the NIST Office of Law Enforcement Standards (OLES) and by the NIST Advanced Technology Program.

\*Note: References are made to certain commercially available products in this paper to adequately specify the experimental procedures involved. Such identification does not imply recommendation or endorsement by the National Institute of Standards and Technology, nor does it imply that these products are the best for the purpose specified. DLP and DMD are trademarks of Texas Instruments, Inc.

## REFERENCES

1. R. O. Green, M. C. Helmlinger, J. E. Conel, and J. van den Bosch, "Inflight validation of the calibration of Airborne Visible/Infrared Spectrometer in 1993," *Proc. SPIE* **2231**, 177-185 (1994).
2. D. K. Clark, M. Feinholz, M. Yarbrough, B. C. Johnson, S. W. Brown, Y. S. Kim, and R. A. Barnes, "Overview of the radiometric calibration of MOBY," *Proc. SPIE* **4483**, 64 (2002).
3. S. Richtsmeier, R. Sundberg, A. Berk, S. Adler-Golden, and R. Haren, "Full spectrum scene simulation," *Proc. SPIE* **5425**, 530-537 (2004).
4. Y. Zong, S. W. Brown, B. C. Johnson, K. R. Lykke, and Y. Ohno, "Simple spectral stray light correction method for array spectrometers," *Appl. Opt.* **45**, 1111-1119 (2006).
5. J. P. Rice, S. W. Brown, and J. E. Neira, "Development of hyperspectral image projectors," *Proc. SPIE* **6297**, 629701 (2006).
6. S. W. Brown, J. P. Rice, J. E. Neira, and B. C. Johnson, "Hyperspectral image projector for advanced sensor characterization," *Proc. SPIE* **6296**, 629602 (2006).

7. J. P. Rice, S. W. Brown, B. C. Johnson, and J. E. Neira, "Hyperspectral image projectors for radiometric applications," *Metrologia* **43**, S61-S65 (2006).
8. S. W. Brown, J. P. Rice, J. E. Neira, B. C. Johnson, and J. D. Jackson, "Spectrally tunable sources for advanced radiometric applications," *J. Res. Natl. Inst. Stand. Technol.* **111**, 401-410 (2006).
9. <http://aviris.jpl.nasa.gov/>
10. J. Gruninger, A. J. Ratkowski, and M. L. Hoke, "The sequential maximum angle convex cone (SMACC) endmember model," *Proc. SPIE* **5425**, 1-14 (2004).